Author Manuscript

Author Manuscript

Author Manuscript

Author Manuscript

HHS Public Access

Author manuscript

Nature. Author manuscript; available in PMC 2010 November 27.

Published in final edited form as:

Nature. 2010 May 27; 465(7297): 478–482. doi:10.1038/nature09001.

Embolus extravasation is an alternative mechanism for cerebral microvascular recanalization

Carson K. Lam[1,*], **Taehwan Yoo**[1,*], **Bennett Hiner**[1], **Zhiqiang Liu**[1], and **Jaime Grutzendler**[1,2,#]

[1]Department of Neurology, Northwestern University Feinberg School of Medicine

[2]Department of Physiology, Northwestern University Feinberg School of Medicine

Abstract

Cerebral microvascular occlusion is a common phenomenon throughout life[1],[2] that could be an underappreciated mechanism of brain pathology. Failure to promptly recanalize microvessels may lead to disruption of brain circuits and significant functional deficits[3]. Hemodynamic forces and the fibrinolytic system[4] are considered the principal mechanisms responsible for recanalization of occluded cerebral capillaries and terminal arterioles. However, using high resolution fixed tissue microscopy and two photon imaging in living mice we found that a large fraction of occluding microemboli failed to be lysed and washed out within 48 hours after internal carotid infusion. Surprisingly, emboli were instead found to translocate outside the vessel lumen within 2-7 days leading to complete re-establishment of blood flow and sparing of the vessel. Recanalization occurred by a previously unknown mechanism of microvascular plasticity involving the rapid envelopment of emboli by endothelial membrane projections which subsequently form a new vessel wall. This was followed by the formation of an endothelial opening through which emboli translocated into the perivascular parenchyma. The rate of embolus extravasation was significantly reduced by pharmacological inhibition of matrix metalloproteinase 2/9 activity. In aged mice, extravasation was markedly delayed, resulting in persistent tissue hypoxia, synaptic damage and cell death. Our study identifies a novel cellular mechanism that may be critical for recanalization of occluded microvessels. Alterations in the efficiency of this protective mechanism may have important implications in microvascular pathology, stroke recovery, and age-related cognitive decline.

Cerebral function and viability are dependent on uninterrupted blood flow through the microvasculature for adequate oxygen and glucose delivery[5]. Thus, robust mechanisms must have evolved to ensure microvascular patency. The fibrinolytic system provides the

Users may view, print, copy, download and text and data- mine the content in such documents, for the purposes of academic research, subject always to the full Conditions of use: http://www.nature.com/authors/editorial_policies/license.html#terms

[#]Corresponding author: Jaime Grutzendler, Northwestern University Feinberg School of Medicine, 303 East Chicago Avenue. Ward 10-132, Chicago, IL 60611, grutzj@northwestern.edu.

[*]These authors contributed equally

AUTHOR CONTRIBUTIONS:

J.G, C.K.L and T.Y conceived and designed the project. C.K.L, T.Y, B.H and J.G performed in vivo two photon imaging. C.K.L, B.H and J.G adapted the technique and performed electron microscopy experiments. C.K.L. and T.Y. performed in situ zymography, aging mice and SB3CT experiments. T.Y performed HUVEC cell culture and imaging experiment. Z.L, C.K.L, T.Y, B.H, and J.G performed histological and confocal microscopy experiments. J.G. wrote the manuscript with significant input from C.K.L and T.Y

Author Manuscript Author Manuscript Author Manuscript Author Manuscript

principal mechanism for degradation of blood clots occluding cerebral blood vessels[4] including terminal arterioles and capillaries[6,7]. Due to their small diameter and relative low flow velocity, microvessels may be prone to occlusion by spontaneously formed microclots as well as detritus not susceptible to fibrinolysis such as fragments of atheromatous plaques[8]. It is not known, if and how blood flow is reestablished when hemodynamic forces and the fibrinolytic system fail to clear occluded microvessels.

To address these questions, we developed a set of tools to visualize the outcome of individual capillary and terminal arteriole occlusions in the mouse brain. Transcranial imaging in living mice with two photon microscopy (TPM)[9] as well as high-resolution confocal and electron microscopy were performed after internal carotid infusion of fluorescently conjugated microemboli (8-20 μm). Although a substantial number of emboli were cleared within 2 hours after infusion presumably by a combined effect of the fibrinolytic system and hemodynamic forces (Supplementary figures 2, 12) a large number of emboli remained in the microvasculature (Figure 1f) and only a modest number were washed out thereafter (Figure 1g). Thus, although fibrinolysis and hemodynamic forces are effective at early clearance of emboli, their efficiency is much lower at later stages. Once retained in the microvasculature, emboli generally caused cessation of blood flow as demonstrated by absence of the characteristic pattern of flowing cells observed in line-scan imaging (Figure 1d, day 1 and Supplementary movie 5).

To determine the outcome of these persistent vessel occlusions, we extended our imaging intervals. As early as two days post-embolization, we were surprised to see that many emboli no longer appeared to be located in the interior of the blood vessels and by day 6 the majority had translocated outside the vessel lumen (Figures 1a-d, h) reestablishing blood flow (Figure 1d, days 3 and 5; Supplementary Movie 2). Given the gradual nature of the extravasation process, it was not possible to image the precise instant of recanalization. However, regardless of when extravasation occurred, in every imaging session in which we saw completely extravasated emboli, flow was already present at the time of imaging (34/34 extravasated fibrin emboli at 2, 3, 5 and 8 days post embolization) suggesting that vessel reflow occurred rapidly. Furthermore, in larger microvessels (~20 μm), which allow flow of multiple rows of cells, reflow was observed even before complete embolus extravasation (Figure 1e; Supplementary Figures 3, 4 and movie 4).

The extravasation phenomenon was observed with fibrin clots (Figures 1a,b,d) as well as substances not susceptible to fibrinolysis such as cholesterol emboli (Figures 1c and 2a) and polystyrene microspheres (Figures 1k; Supplementary movie 3). In vivo imaging in mice expressing endothelial-specific GFP (Tie2-GFP) demonstrated the extravascular location of emboli (Figures 1a-c; 2a-d). This was further confirmed by confocal imaging in tissues immunolabeled for endothelial PECAM-1 and extracellular matrix protein collagen IV (Supplementary Figure 6). Transmission electron microscopy (TEM) demonstrated fibrin clots and microspheres outside of the microvascular lumen and surrounded by processes of perivascular cells (Figure 1i-k). The pattern of clot extravasation was variable with fibrin clots having a tendency to extravasate in smaller fragments (~3-10 μm) (Figure 1d) though many times in larger pieces (Figures 1a,b), while cholesterol emboli generally extravasated with minimal fragmentation (Figures 1c and 2a)

Author Manuscript Author Manuscript Author Manuscript Author Manuscript

Several mechanisms could explain the translocation of embolic material outside the vessel lumen. One possibility is that it occurs by mechanisms similar to the translocation of leukocytes through the blood brain barrier (BBB)[10,11]. Alternatively, endothelial cells near the occlusion may degenerate, allowing the passage of embolic fragments through the vessel which is then repaired by endothelial proliferation. This, however, was ruled out given the absence of immunolabeling with the cell death marker caspase-3 (0/ 35 occluded microvessels in 3 mice) or proliferation marker bromodeoxyuridine (BrdU) (0/73 occluded vessels in 7 mice).

To determine the precise cellular events involved in embolus extravasation, we obtained in vivo time lapse images of fibrin and cholesterol emboli as they underwent extravasation in Tie2-GFP mice. To our surprise, regardless of the composition of the embolic material, we found that within 24-48 hours, the endothelium generated membrane projections that completely enveloped the adjacent emboli (Figures 2a-d; Supplementary movie 1 and figure 13). In some cases the new endothelial membrane was in close contact with the opposing endothelium (Figure 2c, day 3) while in others they appeared to form a narrow lumen (Figure 2d, day 3). TEM confirmed the presence of endothelial membrane projections covering entire emboli (Figures 2e-j), which in some cases were found in contact with the opposing endothelium (Figures 2e,g) forming cell-cell adhesion structures (Figures 2f and h) resembling adherens junctions[12]. In other cases, endothelial membranes appeared separate from each other forming a proto-lumen (Figures 2i and j) similar to what we observed by in vivo imaging (Figure 2a,b and d). This suggests a sequence of events in which frequently the newly formed endothelial membranes make transient adhesion with the opposing endothelium. This is followed by gradual separation after dissociation of cell-cell junctions and possibly by formation of coalescing endothelial vesicles (Figure 2h) similar to what occurs during lumen formation in the developing vasculature[13]. Transient cell adhesion may help in guiding the movement of the endothelial membrane projections while minimizing pathological plasma leakage during the extravasation process.

Once emboli are enveloped, their final movement into the parenchyma requires disruption of the original endothelium to allow their passage. In vivo imaging in Tie2-GFP mice demonstrated that as membrane projections are being formed, the original endothelium undergoes remodeling in what appears to be a retraction process (Figures 2a-d) creating a path for embolus translocation (Figure 2a). It is however, not clear if these endothelial changes are due to the formation of a large transcellular channel or if they occur by disruption of interendothelial tight junctions, both of which have been proposed as mechanisms of leukocyte transmigration[10,14 11]. Given that tight junction (TJ) protein Zonula Occludens-1 (ZO-1) is reduced in microvascular areas adjacent to clots (Figures 2k, l), TJ disruption may be involved in the final endothelial breach prior to extravasation. Although it is not clear what forces drive the final extrusion of emboli, hemodynamic pressure as well as focal microvascular constriction mediated by pericytes[15] could be involved given that we find increased pericyte NG2 immunofluorescence near emboli (Supplementary Figure 7).

In addition to extravasation of whole emboli, we frequently observed that even as fibrin clots were being lysed and washed-out early post embolization, many microvessels retained

Author Manuscript Author Manuscript Author Manuscript Author Manuscript

small fragments from the original clot. These fragments were also enveloped by the membrane of endothelial cells while additional fragments appeared to have already extravasated (Supplementary figure 8). In contrast to extravasation of whole emboli, this phenomenon of fragment engulfment occurs in the first few days after occlusion. Thus, it is possible that smaller scale extravastion can act synergistically with hemodynamic forces and the fibrinolytic system in the early stages of occlusion to accelerate clot dislodgment and wash-out in microvessels.

The process of envelopment and extravasation of emboli is likely to involve complex cellular and molecular events which may include degradation of TJ proteins, adherens junctions and extracellular matrix. Matrix metalloproteinases (MMPs) have been shown to be capable of disrupting these structures[16] and have been implicated in guidance, lumen formation and barrier function in developing blood vessels[17].. Therefore, we investigated the role of MMPs in the extravasation process by measuring MMP 2/9 activity as reflected by tissue gelatinolytic activity using in situ zymography. Interestingly, we found prominent MMP 2/9 activity in areas immediately adjacent to emboli (Figures 3a-c). This activity may originate from adjacent endothelial and perivascular cells such as pericytes which have been shown to secrete MMPs[18]. To further characterize the role of MMPs in the extravasation process, we treated fibrin clot and microsphere embolized mice with MMP 2/9 inhibitor SB-3CT and found a marked reduction in their extravasation (Figures 3d,e and Supplementary figure 9). Thus, MMP 2/9 appear to be important in mediating focal proteolytic events which significantly impact the rate of embolus extravasation.

We subsequently addressed the impact of microvessel occlusion and recanalization on the structure and viability of blood vessels and surrounding neurons. Microsphere embolization in 4 month-old mice led to tissue hypoxia as detected by the pimonidazole hydrochloride technique (hypoxyprobe). Hypoxia was limited to the endothelium and parenchyma generally <100 μm from the occlusion site (Figure 4a) and disappeared following vessel recanalization. Occlusion was associated with little vascular degeneration (Figure 4f and Supplementary figure 5) after embolization with 15 μm microspheres (but none with 10 μm microspheres). Although no obvious synaptic abnormalities were observed with synaptophysin immunolabeling (Figure 4c, young); quantification of dendritic spines in mice expressing yellow fluorescent protein (YFP) in neurons demonstrated a focal reduction in spine density which recovered as vessels reestablished blood flow (Supplementary figure 10). Thus, sufficient redundancy exists in the cerebral microvasculature that occlusion of a single capillary or precapillary arteriole may only induce sufficient hypoxia to cause local transient synaptic pruning but not cell death.

In contrast, 22 month-old mice showed significantly more persistent hypoxyprobe labeling (Figure 4b) and frequently developed dystrophic synapses as detected by synaptophysin labeling (Figures 4c,d) as well as marked increase in caspase-3 immunoreactive perivascular cells (Figures 4e,f). Importantly, aged mice demonstrated a significantly reduced rate of emboli extravasation (Figures 4g,h). Given that extravasation is an active process requiring remodeling of the endothelium and extracellular matrix, age-related cellular alterations as well increased basal lamina thickness and collagen deposition[19] may explain the reduced extravastion. The increased susceptibility to hypoperfusion-induced injury observed in aging

Author Manuscript Author Manuscript Author Manuscript Author Manuscript

may be partly due to reduced extravasation rate coupled to a diminished efficiency in compensatory mechanisms to increase blood flow and an overall greater cellular vulnerability to hypoxia. Reduced extravasation in aging may ultimately lead to capillary loss and decrease in vascular reserve, further augmenting the susceptibility to microvascular occlusion.

Our data describe a previously unknown mechanism of vascular plasticity that leads to recanalization of occluded cerebral microvessels when fibrinolysis and hemodynamic forces fail (Supplementary figures 1, 2 and 14). This mechanism is likely to be essential for clearing emboli composed of materials such as cholesterol or complex blood clots that are not susceptible to fibrinolysis and may thus be critical for tissue reperfusion after thromboembolic stroke. This is consistent with the fact that MMP2/9 inhibitors, which delay extravasation, have been shown to worsen outcome in stroke[20].

Although transient occlusion of large cerebral vessels is known to cause synaptic damage[21], we demonstrate that occlusion of microvessels, though only affecting the blood flow of a few branches downstream[22], can still cause sufficient hypoxia to induce transient focal dendritic spine loss (Supplementary figure 10). In aging, this leads to more severe synaptic injury and perivascular cell death, which could be of special relevance given that age-related structural vascular changes[19] and reduced efficiency of the fibrinolytic system[23] may make the microvasculature prone to occlusion. Delayed extravasation could thus constitute an independent mechanism of cerebral pathology and it may also contribute to cognitive deterioration in Alzheimer's patients with co-morbid conditions affecting the microvasculature such as chronic hypertension, diabetes and amyloid angiopathy[24],[25].

While a normal BBB is essential for maintaining the chemical homeostasis of the brain and abnormalities in the BBB may worsen the outcome of ischemic stroke[26] or lead to neurodegeneration[27],[28], our results demonstrate that a spatially and temporally regulated mechanism of microvascular plasticity leads to a breach in the BBB that serves an important protective role. Improvements in our understanding of this vascular mechanism could lead to therapeutic strategies aimed at preventing age-related cognitive decline and mitigating the consequences of cerebral microembolisms[29]. This mechanism may also be important for recanalization of the microvasculature outside of the cerebral circulation.

Methods summary

To induce cerebral embolization fluorescently conjugated fibrin clots, cholesterol emboli (8-20 μm in diameter) or polystyrene microspheres (10 or 15 μm in diameter) were infused through the mouse internal carotid artery. Emboli were imaged in fixed tissues by confocal microscopy after vessel labeling by intravenous (I.V.) injection of FITC-*lycopersicom esculentum*, thioflavin-S or immunolabeled with anti-PECAM-1, collagen IV or ZO-1 antibodies. Emboli were also imaged overtime in vivo by transcranial two-photon microscopy (TPM) in mice expressing GFP in endothelial cells (Tie2-GFP and ACTB-eGFP) or wild type mice injected I.V. with thioflavin-S. Blood flow velocity was recorded by line scan TPM imaging to verify microvascular occlusion and reestablishment of flow. Transmission electron microscopy was obtained after injection of fibrin emboli conjugated

Author Manuscript Author Manuscript Author Manuscript Author Manuscript

to electron dense colloidal carbon. Quantification of extravasation efficiency was performed from confocal images in fixed brain slices and in a subset of experiments from in vivo TPM time-lapse images. Matrix metalloprotease 2/9 (MMP2/9) activity was measured in areas adjacent to emboli using fluorescent in situ zymography methods. SB-3CT was administered to selectively inhibit MMP2/9 activity and determine the role of MMPs in the extravasation process. Perivascular hypoxia was detected by administration and immunohistochemical detection of hypoxyprobe. Dendritic spine density was quantified in confocal image stacks of fixed brain slices from mice expressing YFP in a subset of pyramidal neurons. Immunohistochemistry of for synaptophysin was used for comparison of synapse-puncta between adult and aged mice.

Full methods

Animals

CB6F1 mice (Jackson Labs) were used for young-aged comparison studies. Tie2-GFP mice (Jackson Labs) were used for in vivo TPM imaging of microvessels. Thy1-YFPH mice (B6.Cg-Tg (Thy1-YFP)16Jrs/J**;** Jackson labs) were used to visualize neuronal processes and quantify dendritic spines. Mice expressing GFP under the CX3CR1 chemokine receptor promoter were used for in vivo imaging of microglia (B6.129P(Cg)-*Ptprc*^{a} *Cx3cr1*^{tm1Litt}/ LittJ ; Jackson labs). Mice expressing eGFP under control of the chicken beta actin promoter (ACTB-eGFP; Jackson labs) were used to visualize cells (leukocytes) flowing within microvessels. All other experiments used CD1 mice. All studies were conducted in mice between 3-5 months old with the exception of aging studies which used 22 month-old mice. Experimental protocols were approved by the Northwestern University Feinberg School of Medicine Institutional Animal Care and Use Committee.

Preparation of emboli

Heterologous fibrin-rich clots were generated by collecting blood from the left ventricle of mice with the same genetic background as the experimental ones. Mouse thrombin (10 μl of 1000 NIH units/mg; Sigma) was added to blood immediately after extraction and incubated at room temperature for 1 hour. Clots were produced with and without cell lysis by rinsing with ddH_2O. To facilitate clot production and minimize the unnecessary sacrifice of mice, experiments requiring a larger number of animals were done with clots generated directly from fibrinogen (Sigma # F8630; 0.6 g/ml in 1XPBS). For either method, fibrin clots were fragmented by sonication and fluorescently conjugated by incubation for 4 hours with Texas Red-X succimydyl ester (1mg/ml in ethanol; Invitrogen). Labeled clot fragments were washed with 70% EtOH and filtered through sieves (8-20μm pore size; Biodesign) and re-suspended in 1XPBS at predetermined concentrations to achieve sparse microvascular occlusion. For detection with transmission electron microscopy, clots were conjugated to colloidal carbon (Higgins, waterproof india ink, passed through a 200 nm. filter)) or polysterene nanoparticles (Duke scientific, 48nm.) by mixing the fibrinogen solution (500 μl) with the carbon or nanoparticle suspension prior to thrombin administration for clot generation. Cholesterol emboli were generated by melting cholesterol crystals (100 mg; Sigma) at 150°C and adding Texas Red-X succimydyl ester to label them fluorescently. The solution was crystallized at room temperature, sonicated in 1XPBS, filtered through sieves

Author Manuscript Author Manuscript Author Manuscript Author Manuscript

(8-20μm pore size) and resuspended. Microsphere emboli were prepared by diluting red fluorescent polystyrene microspheres (10 or 15 μm) (1.25×10^4 microspheres/ml; EZ-Trac, IMT/Stason) in 1XPBS at predetermined concentrations.

Embolization Surgery

Mice were anesthetized by either intraperitoneal injection of ketamine/xylazine (120mg/mL/ 10mg/mL) or inhaled isoflurane. A ventral midline incision was made in the neck to gain access to the left common carotid artery (CCA). The CCA was separated from surrounding connective tissue and blood flow was interrupted by means of retracting sutures. The left external carotid was clamped with temporary ligating sutures to divert emboli into the cerebral circulation via the left internal carotid artery. A small incision was made in the CCA with fine microsurgical scissors and a custom made catheter attached to a Hamilton syringe filled with 200 μl of solution containing emboli at the desired concentrations was inserted into the CCA. All types of emboli were infused over a ~2 minute period. The catheter was removed and the incision was resealed with cyanoacrylate glue (Scotch). Ligating sutures were removed and CCA patency was confirmed by observation of adequate blood filling and CCA pulsations. The surgical wound was sutured and mice were carefully monitored post-operatively.

In vivo two-photon imaging

Anesthetized mice previously infused with emboli were injected through the tail vein with ~100 μl of Thioflavin-S (1% in 0.5% PBS; Sigma), Rhodamine-B dextran (1% in 1XPBS; Invitrogen) or Clear Blue dye (Risk reactor) to label the cerebral vasculature. A midline scalp incision was made and an imaging window was created above the somatosensory cortex by thinning ~700μm diameter skull area with a high-speed drill (Fine Science Tools) as previously described[9], followed by skull immobilization by attachment to a stainless steel plate. Before two-photon imaging, the precise location of emboli was mapped by taking a digital image of the surface microvasculature and respective emboli under fluorescence microscopy. A two photon microscope (Prairie technologies) was used for in vivo imaging. The Ti-sapphire laser (Coherent Inc.) was tuned to 890 nm for simultaneous imaging of microvessels and emboli. Images were taken using a water immersion objective (Olympus 40x, 0.8 N.A.) at a z-step of 1 μm and zoom of 1-4x. Blood flow velocity was recorded in individual cortical microvessels using line scan imaging of flowing blood cells and fluorescent intravascular dye as previously described[30]. After imaging, the skull plate was removed and the scalp incision was closed with 6-0 nylon sutures (Ethicon). The animal was placed back into its cage and monitored until the next imaging time point.

Quantification of emboli retention, washout and extravasation

1) *Early washout (embolus retention)*: ~1500 fibrin or cholesterol emboli were infused through the internal carotid artery. Two hour post embolization mice were sacrificed and postfixed with 4%PFA without cardiac perfusion to avoid perfusion-induced embolus washout. Brain vibratome sections (100 μm) were obtained and imaged with fluorescence microscopy. The total number of emboli in the brain was estimated by counting number of emboli within a sample of 5 representative slices per animal and extrapolating the total

Author Manuscript Author Manuscript Author Manuscript Author Manuscript

number of emboli in the brain taking into account the total number of slices in the forebrain. Data are reported as absolute number of emboli counted. 2) *Delayed washout:* mice were injected with ~1500 fibrin or cholesterol emboli and processed in the same way as described above. Mice were sacrificed at various time points ranging from 2 hours to 6 days. The absolute number of remaining emboli was calculated at each time point and subtracted from the results obtained from the number of emboli remaining at 2 hours postembolization. Washout was plotted as the percentage change overtime of emboli remaining in the brain. 3) *Extravasation:* Mice were embolized with fibrin, cholesterol or polystyrene emboli. Prior to sacrifice, cerebral vasculature was labeled by I.V. injection of fluorescently-conjugated lectin lycopersicom esculentum (100 μl ,1mg/ml; Vector laboratories). Brain slices (50 μm) were obtained with a vibratome and imaged with confocal microscope to quantify extravasation. Emboli were classified by whether they remained within the lumen or were outside of it. Extravasation rate was calculated as the number of extravasation events divided by the total number of clots counted in all brain slices. Quantification of extravasation efficiency using microspheres eliminates the potential bias caused by extravascular degradation, fibrinolysis or washout of clots and the ambiguity encountered when categorizing partially extravasated clots into extravasated or non-extravasated categories. Furthermore, microsphere size and shape are very uniform allowing accurate comparisons between aged and young mice or pharmacologically treated mice.

Measurement of extravasation in MMP 2/9 inhibitor injected mice

Mice embolized with either fibrin clots or microspheres were injected daily (intraperitoneally) with selective MMP 2/9 inhibitor SB-3CT (2mg/ml in 20% DMSO/ ddH_2O; Biomol). Microsphere-embolized mice were treated daily with saline or SB-3CT at 2, 10, and 20 mg/kg/day or acutely with 40mg/kg. Clot-embolized mice were given saline or SB-3CT at 20mg/kg/day. Mice were sacrificed at 4 days post-embolization for clots and 14 days post-embolization for microspheres because of their different time courses of extravasation.

In situ zymography

Brains were harvested at various intervals postembolization with clots or microspheres and rapidly frozen without fixation. Tissues were cryosectioned (20 μm thick) and embedded in fluorescein conjugated *DQ* gelatin from pig skin (15 mg/ml, Invitrogen) for 15 minutes at 4°C and then for 5 hours at 25°C. Tissues were then rinsed with PBS and fixed with 4% paraformaldehyde followed by confocal imaging and fluorescence quantification.

Immunohistochemical labeling

Brain tissue was extracted after perfusion and post-fixed with 4% paraformaldehyde in 1XPBS, cryosectioned, and blocked with 3% normal goat serum /0.1% triton-X100. Incubation with primary antibodies was carried out overnight at 4°C. The primary antibodies used were: collagen IV (Abcam), BrdU (AbD Serotec), NG2 chondroitin (Chemicon), Hypoxyprobe (Chemicon), ZO-1 (Invitrogen), synaptophysin (Chemicon), CD31(PECAM-1) (BD Pharmigen), and IBA1 (Wako). For hypoxia detection, Hypoxyprobe (60mg/kg; Chemicon) was injected intraperitoneally into embolized mice 2

Author Manuscript Author Manuscript Author Manuscript Author Manuscript

hours before sacrifice. To detect cell proliferation, BrdU (40mg/kg; Sigma-Aldrich) was injected intraperitoneally every 24 hours post-embolization until sacrifice.

Fluorescence quantification

ZO-1, NG2, hypoxyprobe and in situ zymography fluorescence was quantified from confocal images of brain slices from embolized mice. A region of interest (ROI) of fixed size was placed centered around the embolus. The average grey scale intensity within this ROI was calculated with NIH Image J software and normalized to fluorescence intensity in multiple control areas measured in adjacent non-occluded microvessels of equal diameter present within the same confocal optical plane. This normalization procedure controls for inter-animal immunolabeling variability and changes fluorescence intensity due to different imaging depths within a confocal stack. Because images in different samples were acquired with the exact same confocal parameters of gain, laser intensity and pinhole and the data is computed as a ratio between the ROI and control areas within the same optical plane, this allows comparison of the ratios rather than absolute fluorescence values between different samples.

Dendritic spine quantification

Thy1-YFPH mice were embolized with 15 μm microspheres, and sacrificed at different time points post-embolization (5 min, day 1, day 7, and day 42). Prior to sacrifice, the intravascular dye thioflavin-S was injected. Confocal imaging of YFP-expressing dendrites in the immediate vicinity of occluded vessels was obtained. Dendrites were segmented into 3 equal portions: area 1 was the intersection between the dendrite and the downstream unperfused portion of the vessel (as determined by reduced intravascular fluorescence); area 2 and area 3 were, respectively, the distal and proximal segments of the dendrite to area 1 and served as internal controls. Spine density was quantified from confocal stacks and normalized as follows:

$$\text{normalized spine density} = \frac{\text{area 1 density}}{\frac{\text{area 2 density} + \text{area 3 density}}{2}}$$

Electron Microscopy

Mice were perfused with a 4% paraformaldeyde and 1% glutaraldehyde solution 7-12 days post-embolization with 10 μm microspheres or 4-8 days postembolization with fibrin clots conjugated to Texas red-X ester (Invitrogen) as well as 48 nm nanoparticles or colloidal carbon (as described above). Coronal brain vibratome (Leica) sections (35 μm) were generated. Diaminobenzidine (DAB; Sigma; 0.06% DAB in a 5% 0.05M Tris buffer at a pH 7.6) was used to photoconvert the fluorescent clots (irradiated at 480 nm wavelength with a 120V mercury lamp). The photoconverted dark clots were located under a dissecting microscope and microdissected with the tip of a 30 gauge needle into ~200 μm diameter pieces containing the occluded vessel. The tissue was processed for electron microscopy using standard methods. Briefly, tissues were immersed in 1% osmium tetroxide for 1 hour at room temperature then dehydrated in an increasing concentration gradient of ethanol. Once fully dehydrated, tissue was transitioned in propylene oxide before transferring into

Author Manuscript Author Manuscript Author Manuscript Author Manuscript

EMBED-812 (Election Microscopy Sciences) overnight. The tissues were placed into an oven at 60°C for 24 hours for polymerization. Embedded tissues were then placed on pre-made epoxy blocks with a drop of resin and placed back in the oven for an additional 24 hours. 70 nm sections were cut on a microtome (Leica), placed on copper grids and allowed to dry for 24 hours at room temperature. Contrast enhancement was achieved by placing the grids on a 4% uranyl acetate solution for 10 minutes followed by 10 minutes in Reynold's lead citrate. Using a JEOL 1220 80 kV transmission electron microscope, copper grids were thoroughly scanned to locate the emboli of interest.

Human vascular endothelial cell culture and live imaging

(HUVEC) cells (courtesy of Dr William Muller, Department of Pathology) were grown on 60mm Poly D lysine treated glass bottom plates in Medium 200 (Invitrogen). Cells were labeled fluorescently by transduction with an AAV virus driving expression of GFP under a CMV promoter. (courtesy of Dr. John Kessler, Department of Neurology). 24 hours after addition of virus, the culture medium was replaced and cells were grown to confluence. 200 uL of Texas-Red conjugated fibrin clots (5000 clots/mL 8-20 um diameter) were added to the plate and allowed to settle for 15 minutes. The plates were kept at 37C on a heating plate and imaged every 15 minutes for 6 hours using two-photon microscopy.

Statistical analysis

All statistical parameters were calculated using Sigma Plot software. Student's t-test was used for most data analysis. For comparison between more than 2 groups, ANOVA test was used. Mann Whitney test was used for comparing the distribution of relative fluorescence intensities of ZO-1 images. A p value <0.05 was considered to be statistical significance.

Supplementary Material

Refer to Web version on PubMed Central for supplementary material.

ACKNOWLEDGMENTS

This work was supported by NIH/NIA grant AG027855 (J.Grutzendler) and a HHMI medical student research fellowship (C.K. Lam). We thank Sharon Lo, Dr. Catarina Freitas, David Choi, and Christina Whiteus for help with experiments. We thank Aaron Schain for suggesting the use of ACTB-eGFP mice and Dr. Enrico Mugnaini for advice with TEM experiments. We also thank Drs. Giovanni D'avossa, Jaime García-Añoveros, John Kessler, and Puneet Opal for helpful discussions and critical review of the manuscript.

CITATIONS

1. Siebler M, Kleinschmidt A, Sitzer M, Steinmetz H, Freund HJ. Cerebral microembolism in symptomatic and asymptomatic high-grade internal carotid artery stenosis. Neurology. 1994; 44:615–618. [PubMed: 7909360]
2. Markus HS, Thomson ND, Brown MM. Asymptomatic cerebral embolic signals in symptomatic and asymptomatic carotid artery disease. Brain. 1995; 118(Pt 4):1005–1011. [PubMed: 7655877]
3. Vermeer SE, et al. Silent brain infarcts and the risk of dementia and cognitive decline. The New England journal of medicine. 2003; 348:1215–1222. [PubMed: 12660385]
4. Collen D. On the regulation and control of fibrinolysis. Edward Kowalski Memorial Lecture. Thrombosis and haemostasis. 1980; 43:77–89. [PubMed: 6450468]

Author Manuscript Author Manuscript Author Manuscript Author Manuscript

5. Powers WJ, Grubb RL Jr. Darriet D, Raichle ME. Cerebral blood flow and cerebral metabolic rate of oxygen requirements for cerebral function and viability in humans. J Cereb Blood Flow Metab. 1985; 5:600–608. [PubMed: 3877067]
6. Levin EG, del Zoppo GJ. Localization of tissue plasminogen activator in the endothelium of a limited number of vessels. The American journal of pathology. 1994; 144:855–861. [PubMed: 8178936]
7. Zlokovic BV, et al. Expression of tissue plasminogen activator in cerebral capillaries: possible fibrinolytic function of the blood-brain barrier. Neurosurgery. 1995; 37:955–961. [PubMed: 8559345]
8. Rapp JH, et al. Atheroemboli to the brain: size threshold for causing acute neuronal cell death. J Vasc Surg. 2000; 32:68–76. [PubMed: 10876208]
9. Grutzendler J, Kasthuri N, Gan WB. Long-term dendritic spine stability in the adult cortex. Nature. 2002; 420:812–816. [PubMed: 12490949]
10. Muller WA. Leukocyte-endothelial-cell interactions in leukocyte transmigration and the inflammatory response. Trends in immunology. 2003; 24:327–334. [PubMed: 12810109]
11. Engelhardt B, Wolburg H. Mini-review: Transendothelial migration of leukocytes: through the front door or around the side of the house? European journal of immunology. 2004; 34:2955–2963. [PubMed: 15376193]
12. Dejana E. Endothelial cell-cell junctions: happy together. Nat Rev Mol Cell Biol. 2004; 5:261–270. [PubMed: 15071551]
13. Kamei M, et al. Endothelial tubes assemble from intracellular vacuoles in vivo. Nature. 2006; 442:453–456. [PubMed: 16799567]
14. Carman CV, Springer TA. A transmigratory cup in leukocyte diapedesis both through individual vascular endothelial cells and between them. The Journal of cell biology. 2004; 167:377–388. [PubMed: 15504916]
15. Peppiatt CM, Howarth C, Mobbs P, Attwell D. Bidirectional control of CNS capillary diameter by pericytes. Nature. 2006; 443:700–704. [PubMed: 17036005]
16. Yang Y, Estrada EY, Thompson JF, Liu W, Rosenberg GA. Matrix metalloproteinase-mediated disruption of tight junction proteins in cerebral vessels is reversed by synthetic matrix metalloproteinase inhibitor in focal ischemia in rat. J Cereb Blood Flow Metab. 2007; 27:697–709. [PubMed: 16850029]
17. Stratman AN, et al. Endothelial cell lumen and vascular guidance tunnel formation requires MT1-MMP-dependent proteolysis in 3-dimensional collagen matrices. Blood. 2009; 114:237–247. [PubMed: 19339693]
18. Page-McCaw A, Ewald AJ, Werb Z. Matrix metalloproteinases and the regulation of tissue remodelling. Nat Rev Mol Cell Biol. 2007; 8:221–233. [PubMed: 17318226]
19. Farkas E, Luiten PG. Cerebral microvascular pathology in aging and Alzheimer's disease. Progress in neurobiology. 2001; 64:575–611. [PubMed: 11311463]
20. Zhao BQ, et al. Role of matrix metalloproteinases in delayed cortical responses after stroke. Nat Med. 2006; 12:441–445. [PubMed: 16565723]
21. Zhang S, Boyd J, Delaney K, Murphy TH. Rapid reversible changes in dendritic spine structure in vivo gated by the degree of ischemia. J Neurosci. 2005; 25:5333–5338. [PubMed: 15930381]
22. Nishimura N, et al. Targeted insult to subsurface cortical blood vessels using ultrashort laser pulses: three models of stroke. Nature methods. 2006; 3:99–108. [PubMed: 16432519]
23. Gleerup G, Winther K. The effect of ageing on platelet function and fibrinolytic activity. Angiology. 1995; 46:715–718. [PubMed: 7639418]
24. Arvanitakis Z, Wilson RS, Bienias JL, Evans DA, Bennett DA. Diabetes mellitus and risk of Alzheimer disease and decline in cognitive function. Archives of neurology. 2004; 61:661–666. [PubMed: 15148141]
25. Iadecola C. Neurovascular regulation in the normal brain and in Alzheimer's disease. Nature reviews. 2004; 5:347–360.
26. Lo EH, Dalkara T, Moskowitz MA. Mechanisms, challenges and opportunities in stroke. Nature reviews. 2003; 4:399–415.

Author Manuscript Author Manuscript Author Manuscript Author Manuscript

27. Abbott NJ, Ronnback L, Hansson E. Astrocyte-endothelial interactions at the blood-brain barrier. Nature reviews. 2006; 7:41–53.

28. Zlokovic BV. The blood-brain barrier in health and chronic neurodegenerative disorders. Neuron. 2008; 57:178–201. [PubMed: 18215617]

29. Pugsley W, et al. The impact of microemboli during cardiopulmonary bypass on neuropsychological functioning. Stroke; a journal of cerebral circulation. 1994; 25:1393–1399.

30. Kleinfeld D, Mitra PP, Helmchen F, Denk W. Fluctuations and stimulus-induced changes in blood flow observed in individual capillaries in layers 2 through 4 of rat neocortex. Proceedings of the National Academy of Sciences of the United States of America. 1998; 95:15741–15746. [PubMed: 9861040]

Author Manuscript Author Manuscript Author Manuscript Author Manuscript

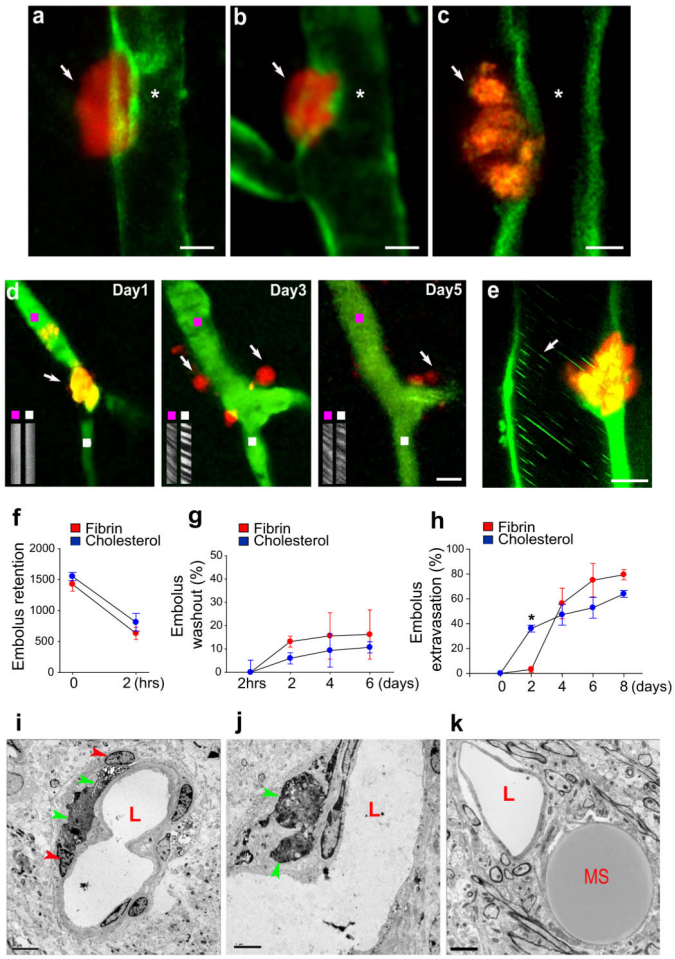

Figure 1. Emboli that fail to be washed-out undergo extravasation leading to blood flow reestablishment

a-c, Single time point transcranial TPM imaging in Tie2-GFP mice show extravasated fluorescent fibrin clots (**a,b** arrows; day 4 post-embolization) and a cholesterol embolus (**c**, arrow; day 3 post-embolization) adjacent to recanalized lumen (asterisk). Scale bars: 10 μm. **d**, Time-lapse imaging shows a capillary (green; Thioflavin-S dye) occluded by a fibrin clot (orange; arrow, day 1), which extravasates and degrades (arrows, days 3 and 5; Supplementary figure 11). Line-scan imaging upstream (purple squares) and downstream (white squares) of the occlusion shows blood flow reestablishment. **e**, In vivo image on day 2 shows a cholesterol embolus in the process of extravasation through the GFP-labeled endothelium (ACTB-eGFP mice). Leukocytes (green lines, arrow) are seen flowing even prior to complete extravasation. **f**, Quantification of fibrin and cholesterol emboli (10-20 μm) retained in the microvasculature which failed to be lysed or washed-out 2 hours post-embolization (~1500 clots per mouse in 12 mice). **g**, Fibrin and cholesterol emboli washout up to 6 days postembolization (mean ± s.e.m. n=3 mice per time point). **h**, Fibrin and cholesterol emboli extravasation up to 8 days post-embolization (mean ± s.e.m.; n=10 mice and 17 fibrin clots and n= 10 mice and 18 cholesterol emboli per mouse). The difference in early extravasation rates between cholesterol and clots (asterisk, $p<0001$) is likely due to a tendency of clots to dislodge from their initial site of occlusion. **i-k**, Transmission electron

Author Manuscript Author Manuscript Author Manuscript Author Manuscript

microscopy (TEM) shows **(i,j)**, colloidal carbon-conjugated fibrin clots (green arrowheads) which have extravasated after 7 days and are surrounded by the processes of perivascular cells (red arrowheads) and (**k)**, a microsphere (MS) outside the capillary lumen (L). Scale bars 5μm.

Author Manuscript Author Manuscript Author Manuscript Author Manuscript

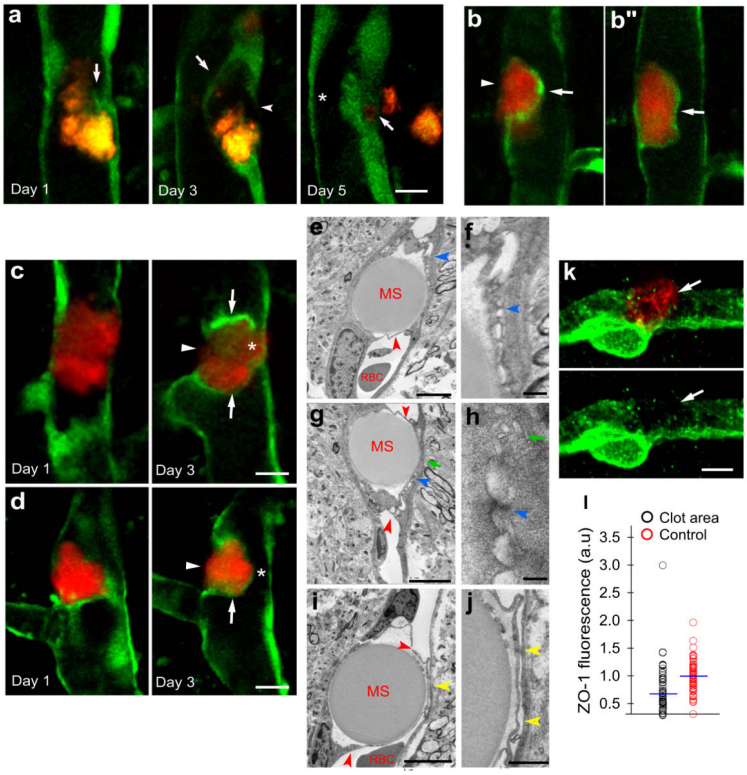

Figure 2. Focal endothelial remodeling underlies the translocation of emboli

a, Time lapse imaging in Tie2-GFP mice shows gradual extension of a membrane from the adjacent endothelium (arrow, day1) eventually surrounding a cholesterol embolus (orange) (arrow, day 3). The original endothelium undergoes retraction (arrowhead, day 3) creating a path for embolus translocation. On day 5, the embolus has extravasated leading to lumen recanalization (asterisk). **b,b"**, Single time point in vivo image shows two optical planes of the same vessel. The fibrin clot (red) is enveloped by a newly formed endothelial extension (arrow) while an opening in the endothelium is visible through which the clot appears to be extravasating (b, arrowhead) (Supplementary Movie 1). **c**,**d**, Time lapse images in Tie2-GFP mice show fibrin clots (red) at different stages in the formation of the endothelial envelope (arrows), endothelial retraction (arrowheads) and lumen reestablishment (asterisks). **e-j**, TEM shows intravascular microspheres which have been enveloped by endothelial extensions (red arrowheads). The newly formed membranes make contact with the opposing endothelium forming specialized cellular junctions (e-h; blue arrowheads) and small vacuolar structures (g,h; green arrows). **(i-j)**, Endothelial membranes are detached from each other and a narrow lumen is apparent (yellow arrowheads). Red blood cells (RBC). **k**, Confocal image of a microvessel immunolabeled for Zonula Occludens-1 (ZO-1) (green) shows reduced labeling (arrows) adjacent to intravascular fibrin clot (red). Scale bar 10μm. **l**, Quantification of ZO-1 immunofluorescence adjacent to clots and control unoccluded microvessels in the same confocal optical plane (n=5 mice and 55 and 57 vessels, $p<0.001$, two-side Mann-Whitney test).

Author Manuscript Author Manuscript Author Manuscript Author Manuscript

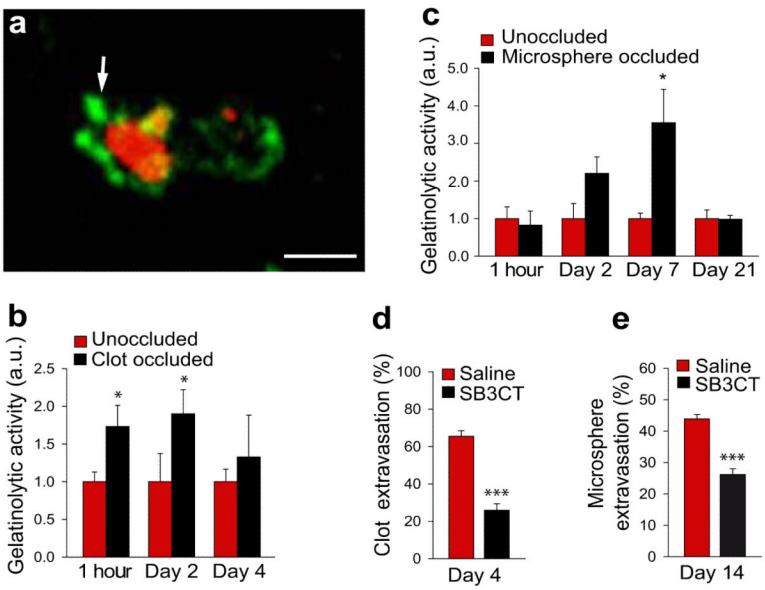

Figure 3. Matrix metalloprotease-2/9 activity is induced around the occlusion site

a, In situ zymography 5 hours post-embolization indicates increased gelatinolytic activity (green) around fibrin clot (red). Scale bar, 10μm. **b-c**, Quantification of gelatinolytic activity around clot **(b)** and microsphere **(c)** occluded microvessels (mean ± s.e.m.; n=35 mice and 110 clot-occluded vessels and n=10 mice and 75 microsphere-occluded vessels. *p<0.05, one-way ANOVA). **d-e**, Quantification of the percentage of extravasated clots **(d)** and microspheres **(e)** in mice treated with MMP 2/9 inhibitor SB-3CT. (mean ± s.e.m.; n=4 mice per treatment group). (***p<0.001 two-tail Student's t-test).

Author Manuscript Author Manuscript Author Manuscript Author Manuscript

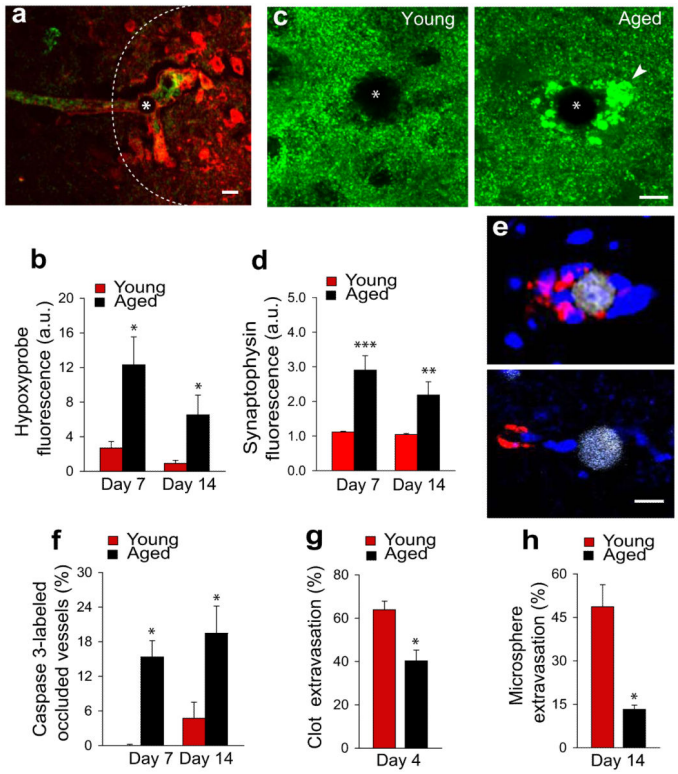

Figure 4. Delayed extravasation in aging contributes to persistent hypoxia, synaptic injury and cell death

a, Occlusion of a microvessel (green lectin) by a microsphere (asterisk) induced focal hypoxia (dotted area) as detected by hypoxyprobe (red). Scale bar 15um **b**, Quantification of hypoxyprobe around microspheres in young and aged mice (mean ± s.e.m.; n=4 mice and 38 blood vessels per group. *p<0.05, two-tail Student's t-test). **c**, Confocal images of synaptophysin-immunoreactivity (green) near occlusion (asterisk) demonstrate enlarged dystrophic synapses (arrowhead) in aged mice. Scale bar 10μm. **d**, Quantification of synaptophysin immunoreactivity shows increased fluorescence in aged mice, reflecting synaptic dystrophy (mean ± s.e.m.; n=11 mice and 147 blood vessels). (**p<0.01 and ***p<0.001, two-tail Student's t-test). **e**, Microspheres occlusion (gray) in aged mice induces caspase-3 immunoreactivity (red) in perivascular cells (blue, DAPI). Scale bar 10μm. **f**, Proportion of vessels that contain caspase-3 immunoreactivity in young and aged mice (mean ± s.e.m.; n=12 mice and 112 blood vessels. *p<0.05, two-tail Student's t-test). **g-h**, Rate of clot **(g)** and microsphere **(h)** extravasation in young adult and aged mice (mean ± s.e.m.; n=6 mice and 45 blood vessels for clots and n=8 mice and 2527 blood vessels for microspheres. *p<0.05, two-tail Student's t-test).